Microwave-Based Structure and Four-Dimensional Morphed Intermolecular Potential for HI−CO_2

Wolfgang Jabs,[†] Fabrice F. Willaert,[†] Blake A. McElmurry,[†] Luis. A. Rivera-Rivera,[†] Raffaele Montuoro,[†] Robert R. Lucchese,[†] John W. Bevan,*[,†] and Richard D. Suenram[‡,§]

Department of Chemistry, Texas A&M University, College Station, Texas 77843-3255, and Optical Technology Division, National Institute of Standards and Technology, Gaithersburg, Maryland 20899

Received: June 7, 2007; In Final Form: July 20, 2007

Microwave spectra of the four isotopologue/isotopomers, HI−$^{12}C^{16}O_2$, HI−$^{12}C^{18}O_2$, HI−$^{12}C^{18}O^{16}O$, and HI−$^{12}C^{16}O^{18}O$, have been recorded using pulsed-nozzle Fourier transform microwave spectroscopy. In the last two isotopomers, the heavy oxygen atom tilted toward and away from the HI moiety, respectively. Only *b*-type $K_a = 1 \leftarrow 0$ transitions were observed. Spectral analysis provided molecular parameters including rotational, centrifugal distortion, and quadrupole constants for each isotopomer. Then, a four-dimensional intermolecular energy surface of a HI−CO_2 complex was generated, morphing the results of ab initio calculations to reproduce the experimental data. The morphed potential of HI−$^{12}C^{16}O_2$ had two equivalent global minima with a well depth of 457(14) cm^{-1} characterized by a planar quasi-T-shaped structure with the hydrogen atom tilted toward the CO_2 moiety, separated by a barrier of 181(17) cm^{-1}. Also, a secondary minimum is present with a well depth of 405(14) cm^{-1} with a planar quasi-T-shaped structure with the hydrogen atom tilted away from the CO_2 moiety. The ground state structure of HI−$^{12}C^{16}O_2$ was determined to have a planar quasi-T-shaped geometry with $R = 3.7717(1)$ Å, $\theta_{OCI} = 82.30(1)°$, $\theta_{CIH} = 71.55(1)°$. The morphed potential obtained is now available for future studies of the dynamics of photoinitiated reactions of this complex.

1. Introduction

There has been considerable interest in using weakly bound binary complexes for investigating the dynamics of elementary chemical reactions.[1] In particular, the following reaction has been extensively studied.[2−9]

$$H + CO_2 \rightarrow [HOCO]^{\ddagger} \rightarrow OH + CO \qquad (1)$$

In such studies, the reactants H and CO_2 have been prepared in situ by photodissociating the HX bond in an $H_nX{:}CO_2$ complex (X = I, Br, Cl, $n = 1$, and X = S, $n = 2$) and the product OH has been probed. As a consequence, these investigations have led to further understanding of the influence of the nearby spectator X atom on such reactions. It has been pointed out that Van der Waals forces as well as large-amplitude zero-point motion of the HX monomer are responsible for governing the initial orientation of the reactants and should be considered in the interpretation of the experimental results. Furthermore, detailed structural studies of the HX:CO_2 complexes (X = F, Cl, and Br)[10−13] have greatly facilitated these interpretations. Microwave studies of CO_2−HCl and CO_2−HF determined linear geometries for these complexes,[10−14] constraining the reaction to be collinear. In contrast, an infrared diode-laser study of the CO_2 asymmetric stretch in HBr−CO_2 concluded that the geometry of the complex is quasi-T-shaped, neglecting the position of the H atom.[12] Such results have been confirmed by a later microwave study that also revealed spectra consistent with a T-shaped Br−CO_2 heavy atom geometry, which consequently affected the reaction dynamics.[13] The quasi-T-shaped geometry observed in HBr−CO_2 is most likely the consequence of the large dispersion interaction between the very polarizable halogen atom and the CO_2, giving a close-packed heavy-atom arrangement. Analogous investigations of the structure of HI−CO_2 have not been available so far, and this has prevented the analysis of regiospecific effects and reaction dynamics for this complex.[4,8,9,15,16]

In this work, we report the microwave spectra of HI−$^{12}C^{16}O_2$, HI−$^{12}C^{18}O_2$, HI−$^{12}C^{18}O^{16}O$, and HI−$^{12}C^{16}O^{18}O$ obtained using pulsed-nozzle Fourier -transform microwave spectroscopy. An optimized model of the intermolecular interaction potential has been generated by morphing the potential energy surface (PES) obtained from ab initio calculations to the measured microwave data. This model has been used to investigate the structure of the complex and to provide new insights into its reactions dynamics.

2. Experimental Section

2.1. Experimental Methods. Spectra were obtained at National Institute of Standards and Technology (NIST) using a Balle−Flygare pulsed-molecular-beam,[17] Fabry−Perot cavity, mini Fourier transform microwave spectrometer, operated in the frequency range between 11 GHz and 20 GHz. Since this instrument has been described previously.[18,19] Only a brief description relevant to the current experiment will be given here. Microwave radiation is coupled to the center of the mirror via a 0.358 cm semirigid coaxial cable. Two commercial pulsed nozzle molecular beam sources have been used on the

* To whom correspondence should be addressed. E-mail: bevan@mail.chem.tamu.edu.

[†] Department of Chemistry, Texas A&M University.

[‡] Optical Technology Division, National Institute of Standards and Technology.

[§] National Institute of Standards and Technollogy, 100 Bureau Drive, Gaithersburg, MD 20899-1070 and Department of Chemistry, University of Virginia, Charlottesville, VA 22904-4319.

10.1021/jp0744275 CCC: $37.00
Published on Web 11/06/2007

TABLE 1: Observed Transition Frequencies in MHz for HI−CO_2 and Isotopomers[a]

J'	F'	J''	F''	HI−$^{12}C^{16}O_2$	HI−$^{12}C^{18}O_2$	HI−$^{12}C^{18}O^{16}O$	HI−$^{12}C^{16}O^{18}O$	J'	F'	J''	F''	HI−$^{12}C^{16}O_2$	HI−$^{12}C^{18}O_2$	HI−$^{12}C^{18}O^{16}O$	HI−$^{12}C^{16}O^{18}O$
1_{10}	3/2	1_{01}	5/2	11433.722	10232.385			3_{12}	9/2	3_{03}	9/2	11979.218	10774.166		
1_{10}	7/2	1_{01}	5/2	11499.963	10298.771			3_{12}	7/2	3_{03}	5/2	12034.677	10830.155		
1_{10}	3/2	1_{01}	3/2	11625.686				3_{12}	9/2	3_{03}	11/2	12092.057			
1_{10}	7/2	1_{01}	7/2	11634.995	10434.128			3_{13}	7/2	2_{02}	7/2	17393.530	15806.783	15258.351	15269.054
1_{10}	5/2	1_{01}	7/2	11780.711	10579.732			3_{13}	9/2	2_{02}	7/2	17395.635	15809.025	15260.459	15271.294
1_{10}	5/2	1_{01}	3/2	11837.639	10636.743			3_{13}	7/2	2_{02}	5/2	17422.377	15835.441	15286.727	15298.178
1_{10}	5/2	1_{01}	5/2		10444.377			3_{13}	5/2	2_{02}	7/2	17445.767		15310.727	
1_{11}	5/2	0_{00}	5/2	13410.093	12081.343	11401.488	11421.068	3_{13}	5/2	2_{02}	5/2	17474.614		15339.105	15350.313
1_{11}	7/2	0_{00}	5/2	13686.201	12357.147	11674.192	11697.509	3_{13}	9/2	2_{02}	9/2	17517.371	15930.822	15380.622	15394.739
1_{11}	3/2	0_{00}	5/2	13806.017	12476.518			3_{13}	3/2	2_{02}	5/2	17535.932			
2_{11}	1/2	2_{02}	3/2	11521.917	10319.455			3_{13}	5/2	2_{02}	3/2	17567.101	15980.514	15430.682	15444.124
2_{11}	9/2	2_{02}	7/2	11567.722	10364.990			3_{13}	11/2	2_{02}	9/2	17607.822	16020.610	15471.144	15484.373
2_{11}	3/2	2_{02}	5/2	11595.957	10393.019			3_{13}	3/2	2_{02}	3/2	17628.418	16041.659		15505.109
2_{11}	1/2	2_{02}	1/2	11603.156				3_{13}	3/2	2_{02}	1/2	17709.656	16122.955	15492.095	
2_{11}	9/2	2_{02}	9/2	11689.458	10486.787			3_{13}	1/2	2_{02}	1/2	17753.085	16165.986	15615.624	
2_{11}	5/2	2_{02}	7/2	11756.721	10553.985			4_{13}	3/2	4_{04}	3/2	11928.333			
2_{11}	3/2	2_{02}	1/2	11769.682	10567.047			4_{13}	5/2	4_{04}	5/2	12027.172			
2_{11}	5/2	2_{02}	5/2	11785.569	10582.644			4_{13}	7/2	4_{04}	7/2	12128.345			
2_{11}	7/2	2_{02}	7/2	11826.419	10623.911			4_{13}	11/2	4_{04}	9/2	12162.561			
2_{11}	7/2	2_{02}	5/2	11855.266	10652.571			4_{13}	11/2	4_{04}	11/2	12177.094	10968.801		
2_{11}	5/2	2_{02}	3/2	11878.056	10675.378			4_{13}	7/2	4_{04}	5/2	12194.394			
2_{11}	7/2	2_{02}	9/2	11948.149	10745.708			4_{13}	9/2	4_{04}	9/2	12194.876			
2_{12}	7/2	1_{01}	5/2	15416.326	13957.962	13345.060	13359.670	4_{13}	9/2	4_{04}	11/2	12209.410			
2_{12}	5/2	1_{01}	5/2	15447.661	13989.027	13376.343	13390.696	4_{13}	9/2	4_{04}	7/2	12236.761			
2_{12}	7/2	1_{01}	7/2	15551.360	14093.317	13478.565	13496.655	4_{13}	11/2	4_{04}	13/2	12282.508			
2_{12}	5/2	1_{01}	7/2	15582.693		13509.846		4_{13}	13/2	4_{04}	13/2	12008.648	10800.201		
2_{12}	5/2	1_{01}	3/2	15639.623	14181.398	13566.157	13585.385	4_{13}	5/2	4_{04}	3/2	12091.897			
2_{12}	9/2	1_{01}	7/2	15674.141	14215.209	13600.986	13618.796	4_{13}	5/2	4_{04}	7/2	11961.122	10752.911		
2_{12}	3/2	1_{01}	3/2	15745.772	14287.904	13672.182	13691.778	4_{14}	9/2	3_{03}	7/2		17573.161	17085.317	17093.212
2_{12}	3/2	1_{01}	5/2	15553.808		13482.367		4_{14}	9/2	3_{03}	9/2			17089.588	17096.561
2_{12}	1/2	1_{01}	3/2	15820.136				4_{14}	11/2	3_{03}	9/2		17584.826	17100.765	17107.701
3_{12}	1/2	3_{03}	3/2	11665.385	14361.185	13746.211		4_{14}	7/2	3_{03}	7/2			17119.456	17127.014
3_{12}	11/2	3_{03}	9/2	11705.633				4_{14}	7/2	3_{03}	9/2		17607.822		
3_{12}	1/2	3_{03}	1/2	11721.148				4_{14}	7/2	3_{03}	5/2		17664.999	17178.010	17186.507
3_{12}	3/2	3_{03}	5/2	11724.040	10519.564			4_{14}	13/2	3_{03}	11/2		17775.117	17290.284	17299.341
3_{12}	3/2	3_{03}	3/2	11796.352	10591.100			4_{14}	5/2	3_{03}	3/2		17788.045	17301.787	
3_{12}	11/2	3_{03}	11/2	11818.468	10613.088			5_{14}	5/2	5_{05}	5/2	12188.861			
3_{12}	5/2	3_{03}	5/2		10690.928			5_{15}	11/2	4_{04}	9/2		19274.447	18854.734	18858.014
3_{12}	5/2	3_{03}	7/2	11837.726	10633.067			5_{15}	13/2	4_{04}	11/2		19304.402	18885.043	18887.973
3_{12}	3/2	3_{03}	1/2	11852.120				5_{15}	9/2	4_{04}	7/2		19341.580		
3_{12}	5/2	3_{03}	3/2	11967.784	10762.463			5_{15}	15/2	4_{04}	13/2		19481.335	19060.994	19066.143
3_{12}	7/2	3_{03}	7/2	11976.927				5_{15}	5/2	4_{04}	3/2		19568.111		
3_{12}	7/2	3_{03}	9/2	11977.884				6_{15}	11/2	6_{06}	11/2	12734.228			
3_{12}	9/2	3_{03}	7/2	11978.261											

[a] Experimental uncertainties on the transitions are estimated to be ±5 kHz (±1σ).

TABLE 2: Spectroscopic Constants[a] for HI−CO_2 and Isotopologues/Isotopomers (in MHz)

	HI−$^{12}C^{16}O_2$	HI−$^{12}C^{18}O_2$	HI−$^{12}C^{18}O^{16}O$	HI−$^{12}C^{16}O^{18}O$
A	12630.3794(13)[b]	11365.09291(83)	10654.1037(25)	10678.3653(27)
B	1087.4242(16)	1020.78971(86)	1053.9091(26)	1050.7627(26)
C	988.07631(54)	923.46000(36)	955.59604(75)	953.15160(77)
Δ_{JK}	0.168020(263)	0.142611(96)		
$eQq_{aa,0}$	639.6916(49)	640.7206(58)	632.8231(70)	649.0339(85)
$eQq_{aa,1}$	641.621(10)	643.039(10)		
$(eQq_{bb}-eQq_{cc})_0$	−552.52(14)	−544.279(22)	−495.8825(28)	−499.9435(37)
$(eQq_{bb}-eQq_{cc})_1$	−498.9821(19)	−498.5682(21)		
$\lvert eQq_{ab}\rvert$	250.65(14)	242.49(10)	275.488(98)	210.52(12)
σ	0.069	0.075	0.024	0.019

[a] Fitted using JPL Program, H. M. Pickett, *J. Mol. Spectrosc.* **1991**, *148*, 371. [b] The numbers shown in parenthesis are Type A uncertainties with $K = 1$ coverage, i.e., 1σ.

spectrometer, with sizes of the orifices from 0.3 to 1 mm and beam pulse lengths extending from 100 μs to 1 ms.

In the present experiments, the gas mixtures are controlled by mass-flow controllers. Typically, one gas mixture consists of HI in Ar and the other of CO_2 in Ar, with the mole fractions of HI and CO_2 varying from 0.5% to several units percent. The data from several hundred nozzle pulses are averaged. Typical linewidths are 15−20 kHz and all frequency measurements are estimated to have an uncertainty less than 5 kHz.

2.2. Results. The measured transitions for the HI−CO_2 isotopomers are listed in Table 1. Only *b*-type, $\Delta K_a = 1$ transitions were observed. The individual rotational transitions split into a number of hyperfine components over a broad range of frequency due to the nuclear quadrupole interactions of the $I = 5/2$ ^{127}I nucleus. Figure 1 shows the hyperfine components of the transition $2_{12} \leftarrow 1_{01}$ of HI−$^{12}C^{16}O_2$. In this case, the nine hyperfine components cover a range of 400 MHz. The spectral features were analyzed by fitting the data to a spectrum

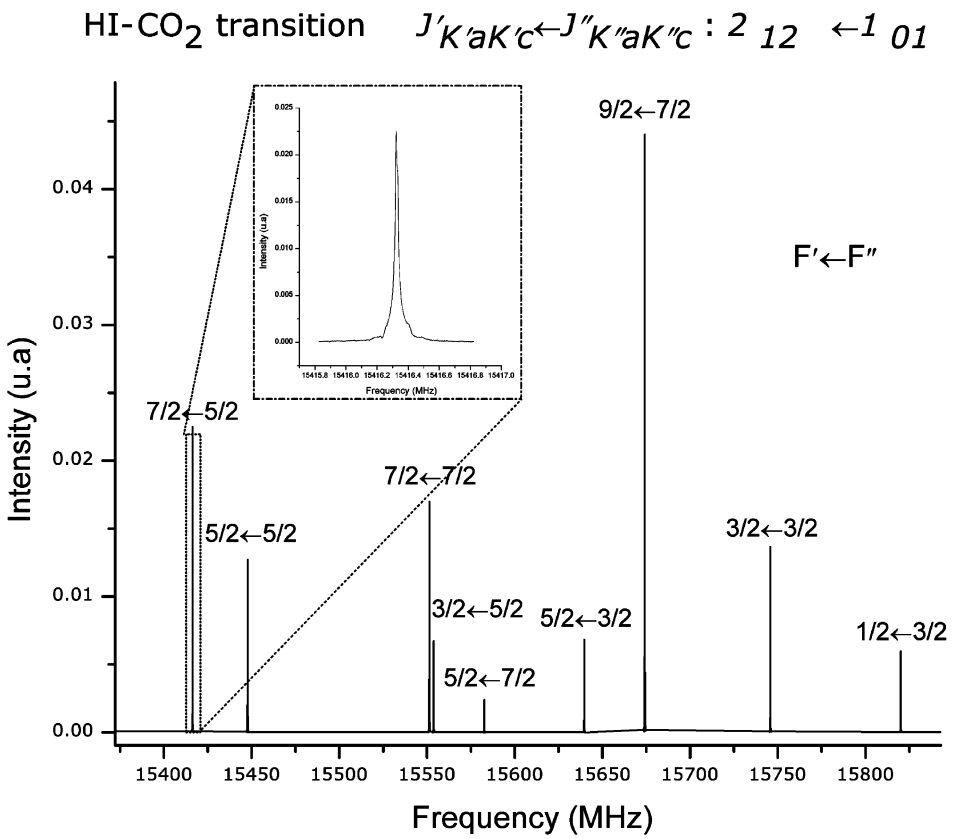

Figure 1. Hyperfine components of the transition $2_{12}\leftarrow1_{01}$ of HI$-{}^{12}C^{16}O_2$.

generated by the Hamiltonian of a rigid asymmetric rotor:[11]

$$H_R = \frac{1}{2}\{(B+C)J^2 + [2A-(B-C)]J_a^2 + (B-C)(J_b^2 - J_c^2)\} \quad (2)$$

The rotational ladders were supplemented by one centrifugal distortion term using the Watson asymmetric-rotor centrifugal-distortion Hamiltonian written in the *A*-reduced I^r representation.[20]

In addition to the rotational Hamiltonian, we also included the ^{127}I nuclear electric quadrupole Hamiltonian H_Q. The quadrupole coupling constant is designated by eQq,[21] and the general expression for the quadrupole coupling energy is

$$E_Q = \frac{2}{(J+1)(2J+3)} \sum_{g=a,b,c} eQq_{gg}(J,i|J_g^2|J,i) \times \left[\frac{\frac{3}{4}C(C+1) - J(J+1)I(I+1)}{2J(2J-1)I(2I-1)}\right] \quad (3)$$

where,

$$C = F(F+1) - J(J+1) - I(I+1)$$
$$F = J+I, J+I-1, J+I-2, ..., |J-I| \quad (4)$$

Spectra of HI$-{}^{12}C^{16}O_2$ and HI$-{}^{12}C^{18}O_2$ showed a larger number of transitions than those of the two mono-^{18}O substituted complexes, HI$-{}^{12}C^{18}O^{16}O$ and HI$-{}^{12}C^{16}O^{18}O$. In fact, for these last two isotopomers, the observed lines can be assigned to pure rotational transitions within the ground vibrational state of an asymmetric top, characterized by the selection rules $\Delta J = 1$ and $\Delta K_a = 1$, with *J* up to 5. On the contrary, in order to assign all the transitions observed in the spectra of the $^{16}O^{16}O$ and $^{18}O^{18}O$ isotopologue complexes, it was necessary to introduce two states into the Hamiltonian (eq 2). However, due to the limited K_a data available, the values of the rotational and centrifugal distortion constants were constrained to be the same for the two states, although each one of those states was characterized by their own set of quadrupole coupling constants eQq_{aa} and $eQq_{bb}-eQq_{cc}$.

As the quadrupole coupling has a large magnitude, the treatment of this interaction required going beyond the usual first-order approximation by adding off-diagonal terms in the asymmetric-rotor nuclear-quadrupole Hamiltonian for both states.

The results from the fittings of the observed transitions are listed in Table 2. The standard deviations of the fits were in the range 19−75 kHz, larger than the experimental precision of ∼5 kHz. The quality of the fits was better for the two mono-^{18}O substituted complexes than that for HI$-{}^{12}C^{16}O_2$ and HI$-{}^{12}C^{18}O_2$.

3. Structural Determination

3.1. Distance *R* (Distance between the Centers of Mass of the Two Monomers). The inertial defects derived from the spectra for the mono-^{18}O substituted complexes are relatively large and positive (1.90 and 1.93 uma·Å^2). Similar values have been found in a number of planar T-shaped complexes,[22−24] where zero-point vibrations in the van der Waals force field gave rise to such positive and relatively large inertial defects.

Figure 2 shows the geometrical parameters *R*, θ_{OCI}, θ_{CIH} (= 180° − θ_{HI}) and ϕ, used in the determination of the structure. The angles θ_{OCI} and θ_{CIH} describe the orientation of both monomers with respect to the axis containing their centers of mass. The dihedral angle ϕ measures the orientation of HI relative to CO_2 in the complex. *R* is the distance between the centers of mass of the two constituents and describes the

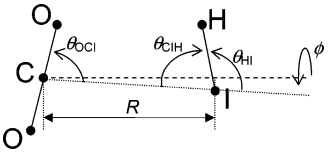

Figure 2. Schematic drawing of HI−CO_2 complex showing the coordinates used.

stretching motion of the complex. Also, *R* depends only on the moment of inertia about the *c*-axis, and can be calculated from[25]

$$\mu R^2 = I_c - I_{HI} - I_{CO_2} \quad (5)$$

where $\mu = M_{HI}M_{CO_2}/(M_{HI} + M_{CO_2})$ is the reduced mass of the complex and I_{HI} and I_{CO_2} are the moments of inertia of the monomers, respectively. The values of μ, I_{HI}, I_{CO_2}, and *R* for all the isotopomers are listed in Table 3.

The *R* values obtained for the ground state geometries of HI−$^{12}C^{16}O_2$, HI−$^{12}C^{18}O_2$, HI−$^{12}C^{18}O^{16}O$, and HI−$^{12}C^{16}O^{18}O$ complexes are 3.7717(1) Å, 3.7699(1) Å, 3.7686(1) Å, and 3.7739(1) Å, respectively. The difference between the first two values give a decrease by 0.0018(2) Å for *R*, which can be attributed to the larger reduced mass of HI−$^{12}C^{18}O_2$ compared to HI−$^{12}C^{16}O_2$. The value of *R* for the mono-^{18}O substituted complexes should be the average of the *R* values of HI−$^{12}C^{16}O_2$ and HI−$^{12}C^{18}O_2$, i.e., 3.7708 Å. For the first mono-^{18}O substituted complex with a *R* value of 3.7686 Å, the difference is −0.0022(2) Å (= 3.7686−3.7708) and for the other one, +0.0031(2) Å (= 3.7739−3.7708). These results indicated that for the first complex, the ^{18}O atom is tilted toward the I atom and for the other mono-^{18}O substituted, the ^{18}O atom is tilted away from the I atom.

3.2. Angle θ_{CIH}. The projection of the HI quadrupole tensor onto the principal inertia axis of HI−CO_2 results in the following equation,[26]

$$eQq_{aa}^{HI-CO_2} = eQq^{HI}\langle P_2(\cos\theta_2)\rangle \quad (6)$$

where $0° \le \theta_2 \le 180°$ is the angle between the HI axis and the *a* principal inertia axis of the complex. The $eQq_{aa}^{HI-CO_2}$ is the component of the quadrupole coupling constant of the complex as measured along the *a*-axis, and eQq^{HI} is the quadrupole coupling of the isolated HI, that is −1828.286(9) MHz.[27] The relatively large mass of the iodine atom permits us to consider the angle θ_2 as approximately equal to the angle θ_{CIH} (Figure 2). To calculate this angle, we used the following approximation: $\langle\cos^2\theta_2\rangle \approx (\cos\theta_2)$.[2] The results for the angle θ_{CIH} are listed in Table 3.

3.3. Angle θ_{OCI}. The angle θ_{OCI} can be determined using the following equation:

$$\sin^2\theta_{OCI} = \frac{I_a(I_c - I_a)}{I_1(I_c - I_1 - I_2)} - \frac{I_2}{I_1}\sin^2\theta_{CIH} - \frac{I_2}{(I_c - I_1 - I_2)}\sin^2(\theta_{OCI} + \theta_{CIH}) \quad (7)$$

In eq 7, the use of the moment of inertia along the *a*-axis gave a value of θ_{OCI} only for the two mono-^{18}O substituted complexes. A detailed discussion of the determination of the angle θ_{OCI} for pure isotopic complexes is presented in Section 5. The results for the angle θ_{OCI} are listed in Table 3.

4. Theoretical Calculations

In this study, we generated a model of the intermolecular potential energy surface of HI−CO_2 by using the potential morphing methodology that was previously employed for the investigation of $(HBr)_2$[28] and OC−HCl[29] complexes. Within this procedure, the ab initio potential energy surface of the HI−CO_2 complex is first obtained. Then, the values of the rotational, centrifugal distortion, and $\langle P_2(\cos\theta_{HI})\rangle$ constants are determined by using the calculated rotational energy levels. These values are compared with the experimentally determined ones and the calculated potential energy surface is iteratively adjusted to reproduce the experimental parameters with the minimum root-mean-square deviation. Each step is described in detail below.

4.1. Ab Initio Calculation of the Intermolecular Potential. The intermolecular potential energy surface was generated by assuming that the geometries of the monomers CO_2 and HI were linear and rigid. In all the calculations, the bond length of HI was fixed at the experimental value $r_e = 1.6092$ Å.[30] The C−O bond length in CO_2 was taken to be $r_e = 1.1625$ Å, which is undistinguishable from the r_0 value within the experimental error.[31] As a consequence of this approximation, the original nine−dimensional (9-D) vibrational model was reduced to a four-dimensional (4-D) model. The interaction potential of HI−CO_2 complex was therefore expressed in terms of the Jacobi coordinates (*R*, θ_{OCI}, θ_{HI}, ϕ), as used in the analysis of the experimental data (Figure 2).[32]

The ab initio interaction energy of the complex was calculated at the coupled cluster singles and doubles with perturbated triples [CCSD(T)] level of theory, within the nonrelativistic approximation, by using the MOLPRO 2006 electronic structure package.[33] The augmented correlation consistent polarized valence triple-ζ basis set (aug-cc-pVTZ)[34,35] was used for all the atoms except for the iodine, for which the basis set was aug-cc-pVTZ-pp.[36] Every calculated point was corrected for the basis set superposition error (BSSE) using the counterpoise correction of Boys and Bernardi.[37] The potential energy surface was calculated on a grid, built taking nine different *R* points (from 3.500 Å to 8.000 Å), five points for both θ_{OCI} and θ_{HI} (from 0° to 180°), and 10 points for ϕ (from 0° to 360°). This set of points was supplemented with a selection of 20 specific angular points (θ_{OCI}, θ_{HI}, ϕ) for each value of *R*, giving a final grid composed of 2430 points. To have a global representation of the surface, the angular dependence of the calculated PES was fitted to a spherical expansion[32] for each value of R_j. A weighting factor $F_w = 75.0$ cm^{-1} was used in order to obtain an absolute average difference less than 6.0 cm^{-1} between the values of the points in the ab initio and fitted potentials for the points within 250.0 cm^{-1} of the minimum of the potential.[32] More details of the fitting procedure have been given elsewhere.[32,38] The 4-D potential was obtained by interpolating the angular potential on the grid of R_j points at fixed angular coordinates using a one-dimensional radial reproducing kernel.[32,38]

The 4-D ab initio PES has two equivalent global minima with well depth of 421.7 cm^{-1} at the geometries $R = 4.000$ Å, $\theta_{OCI} = 73.8°$, $\theta_{HI} = 120.3°$, $\phi = 0.0°$, and $R = 4.000$ Å, $\theta_{OCI} = 106.2°$, $\theta_{HI} = 120.3°$, $\phi = 180.0°$.

4.2. Calculation of Rotational Energy Levels. The rotational energy levels were calculated using the 4-D PES by the pseudospectral approach, discussed previously.[32,38] The experimental value of the rotational constants B_0 for the isolated monomers were used in the expression of the kinetic energy for all the calculations.[39,40] The accuracy of the resulting eigenvalues was controlled by the following parameters:[32] $R_{start} = 3.500$ Å (the first point of the radial grid), $R_{end} = 8.000$ Å (the last point), $N_R = 38$ (the number of grid points in the radial direction), $N_{\theta OCI} = 48$ and $N_{\theta HI} = 24$ (the numbers of θ_{OCI} and

TABLE 3: Structural Parameters for HI−CO_2 and Its Isotopologues/Isotopomers

	HI−$^{12}C^{16}O_2$	HI−$^{12}C^{18}O_2$	HI−$^{12}C^{18}O^{16}O$	HI−$^{12}C^{16}O^{18}O$
μ (uma)	32.73281	34.90168	33.82974	33.82974
I_{HI} (uma·Å^2)[a]	2.62463594(26)			
I_{CO_2} (uma·Å^2)[b]	43.200165(8)	48.606358(14)	45.785466(12)	45.785466(12)
I_C (uma·Å^2)	511.47386(27)	547.23960(36)	528.85945(42)	530.21576(43)
R (Å)	3.771714(38)	3.769924(30)	3.768557(58)	3.773873(57)
$eQq_{aa}^{HI-CO_2}$ (MHz)	639.6916(49)	640.7206(58)	632.8231(70)	649.0339(85)
θ_{CIH} (deg)	71.55(1)	71.59 (1)	71.32 (1)	71.89(1)
θ_{HI} (deg)	108.45(1)	108.41(1)	108.68(1)	108.11(1)
θ_{OCI} (deg)	82.30(1)[c]	82.51(1)[c]	82.15(1)	82.56(1)

[a] From ref 27. [b] From ref 35. [c] Estimated value (discussed in Section 5).

TABLE 4: Experimental Data Used in the Fits and Fitted Values with the Uncertainties Used

isotopomer	observable	units	$V_{ab\ initio}$	$V_{morphed}$	exp	σ_k
HI−$^{12}C^{16}O_2$	A	cm^{-1}	0.459	0.416	0.421	0.003
	$(B+C)/2$	10^{-2} cm^{-1}	3.191	3.462	3.462	0.002
	Δ_{JK}	10^{-8} cm^{-1}	2325.8	520.0	560.5	10.0
	$\langle P_2(\cos\theta_{HI})\rangle$ (HI)		−0.317	−0.351	−0.350	0.001
HI−$^{12}C^{18}O_2$	A	cm^{-1}	0.414	0.374	0.379	0.003
	$(B+C)/2$	10^{-2} cm^{-1}	2.989	3.243	3.243	0.002
	Δ_{JK}	10^{-8} cm^{-1}	2483.8	520.4	475.7	10.0
	$\langle P_2(\cos\theta_{HI})\rangle$(HI)		−0.316	−0.351	−0.350	0.001
HI−$^{12}C^{18}O^{16}O$	A	cm^{-1}	0.362	0.358	0.355	0.003
	$(B+C)/2$	10^{-2} cm^{-1}	3.093	3.354	3.351	0.002
	$\langle P_2(\cos\theta_{HI})\rangle$(HI)		−0.309	−0.345	−0.346	0.001
HI−$^{12}C^{16}O^{18}O$	A	cm^{-1}	0.363	0.360	0.356	0.003
	$(B+C)/2$	10^{-2} cm^{-1}	3.084	3.340	3.342	0.002
	$\langle P_2(\cos\theta_{HI})\rangle$(HI)		−0.324	−0.357	−0.355	0.001
	G		101.50	1.96		

TABLE 5: Optimized Values for the Parameters of the Morphing Functions

α	i	$\lambda_{\alpha,i}=(l_x$	n	θ_{OCI}	θ_{HI}	$\phi)$	$C^0_{\alpha,i}$	$C_{\alpha,i}$	σ
1	1	0					1.0	1.0433	0.0084
2	1	0					1.0	(1.0)	constrained
3	1	0					0.0	0.03804	0.00017
1	2	2	2	90	90	0	0.0	0.2181	0.0039

TABLE 6: Predicted Spectroscopic Constants Form the Morphed Potential for DI−$^{12}C^{16}O_2$

observable	units	value
A	cm^{-1}	0.361
$(B+C)/2$	10^{-2} cm^{-1}	3.460
$\langle P_2(\cos\theta_{DI})\rangle$(DI)		

θ_{HI} points used in the grid), and $N_\phi = 54$ (the number of ϕ points). The number of radial functions and radial spectral basis functions is $N_F = 34$. All of the summations over spectral states are truncated so that $j_{CO_2} \le j_{max} = 26$ and $j_{HI} \le j_{max} = 22$ include all possible values of m_{CO_2} and m_{HI}. The tolerance used to determine the convergence of the eigenvalues in the Lanczos procedure was 10^{-12}.

4.3. Morphing the Ab Initio Potential. The ab initio potential, $V_{ab\ initio}(R, \theta_{OCI}, \theta_{HI}, \phi)$, was morphed using the transformation

$$V_{morphed}(R, \theta_{OCI}, \theta_{HI}, \phi) = S_1(\theta_{OCI}, \theta_{HI}, \phi) \times V_{ab\ initio}(S_2(\theta_{OCI}, \theta_{HI}, \phi)(R - R_F) + [1 + S_3(\theta_{OCI}, \theta_{HI}, \phi)]R_F, \theta_{OCI}, \theta_{HI}, \phi) \quad (8)$$

where,

$$S_\alpha(\theta_{OCI}, \theta_{HI}, \phi) = \sum_i C_{\alpha,i} F_{\lambda\alpha,i}(\theta_{OCI}, \theta_{HI}, \phi) \quad (9)$$

In eq 9, $C_{\alpha,i}$ are the morphing parameters and F_λ are the angular morphing functions[28,29] labeled by the index $\lambda = (l_x, n, \theta'_{OCI}, \theta'_{HI}, \phi')$. In this work, we used $n = 2$ and angular morphing functions with $l_x = 0$ and 2. The morphing functions are then given by

$$F_\lambda(\theta_{OCI}, \theta_{HI}, \phi) = [N_\lambda \sum_{l_{OCI}=0}^{l_x} \sum_{l_{HI}=0}^{l_x} \sum_{m=-\min(l_{OCI},l_{HI})}^{\min(l_{OCI},l_{HI})} I_{l_{OCI},l_{HI},m}(\theta_{OCI}, \theta_{HI}, \phi) I_{l_{OCI},l_{HI},m}(\theta'_{OCI}, \theta'_{HI}, \phi')]^n \quad (10)$$

The value of N_λ is chosen so that $F_\lambda(\theta'_{OCI}, \theta'_{HI}, \phi') = 1$. The F_λ are defined so that they approach Dirac delta functions located at $(\theta'_{OCI}, \theta'_{HI}, \phi')$ as l_x increases with $n = 1$. In the present study, the value of R_F was selected to be 3.900 Å. The morphing parameters were obtained by a regularized nonlinear least-squares optimization[41] using the regularization parameter $\gamma = 10.0$. The quality of the fit of the experimental data was evaluated by computing the value of the root-mean-square (rms) deviation from the experimental data

$$G(\gamma) = \left[\frac{1}{M}\sum_{k=1}^{M}\left\{\frac{O_k^{expt} - O_k^{calc}(C_{\alpha,i}(\gamma))}{\sigma_k}\right\}^2\right]^{1/2} \quad (11)$$

4.4. Results. The experimental data used to morph the PES of HI−CO_2 complex are reported in Table 4. The PES was morphed using three morphing functions, two with no angular dependence ($l_x = 0$) and one localized angular function with l_x

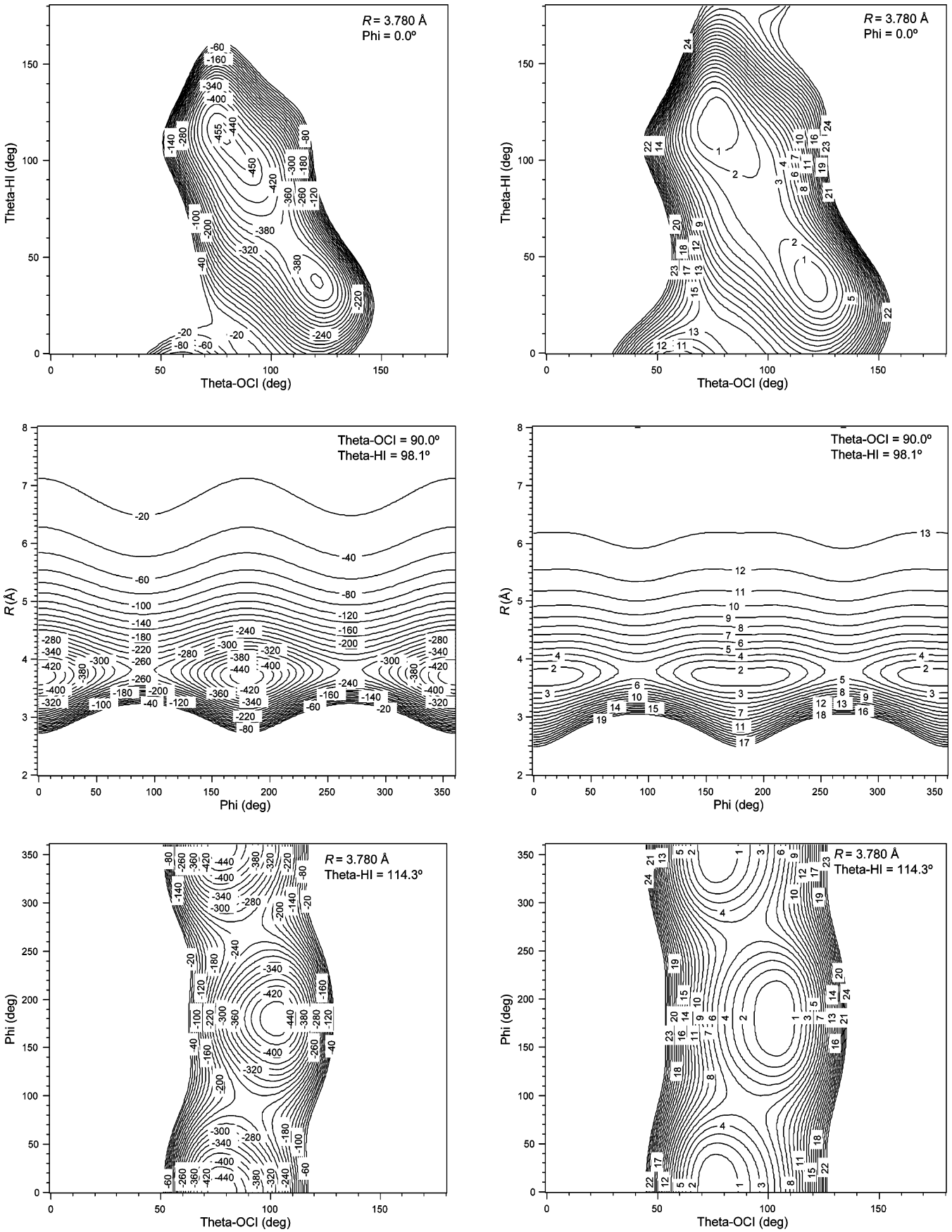

Figure 3. Morphed potential of HI−$^{12}C^{16}O_2$ (left side of the figure) with the corresponding statistical uncertainties (right side of the figure), relative to the minimum of the potential which occurs at $R = 3.780$ Å, $\theta_{OCI} = 77.9°$, $\theta_{HI} = 114.3°$, and $\phi = 0.0°$, with $V = -457(14)$ cm^{-1}. All contours are given in cm^{-1}.

$= 2$ (Table 5). During the fitting procedure, the morphing parameter $C_{2,1}$ was not included as it could not be determined with statistical significance and did not change the quality of the final fit. The final rms after the morphing was $G = 1.96$

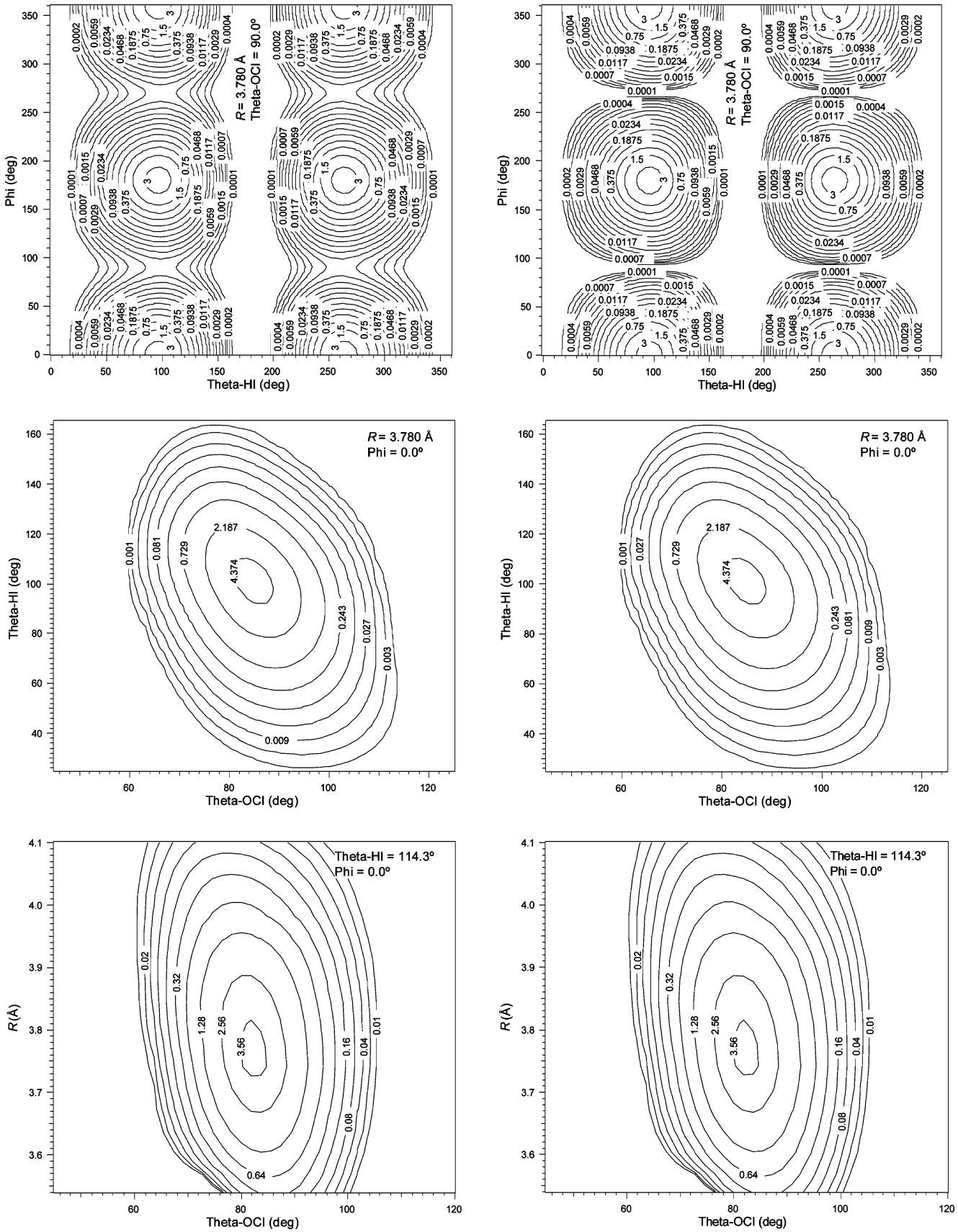

Figure 4. Probability densities of HI$-^{12}C^{16}O_2$ in the ground state (left side of the figure) with energy of $E = 340.954$ cm^{-1} and in the first excited state (right side of the figure) with energy of $E = 340.917$ cm^{-1}. All contours are given in arbitrary units.

and indicates an improved agreement with the experimental data when compared to the original ab initio data with $G = 101.50$.

In Figure 3, two-dimensional slices of the morphed potential of HI$-^{12}C^{16}O_2$ are shown in the left column and the corresponding estimated errors relative to global minimum are shown in the right column. Two equivalent global minima with a well depth of 457(14) cm^{-1} were determined, corresponding to the geometries $R = 3.780$ Å, $\theta_{OCI} = 77.9°$, $\theta_{HI} = 114.3°$,

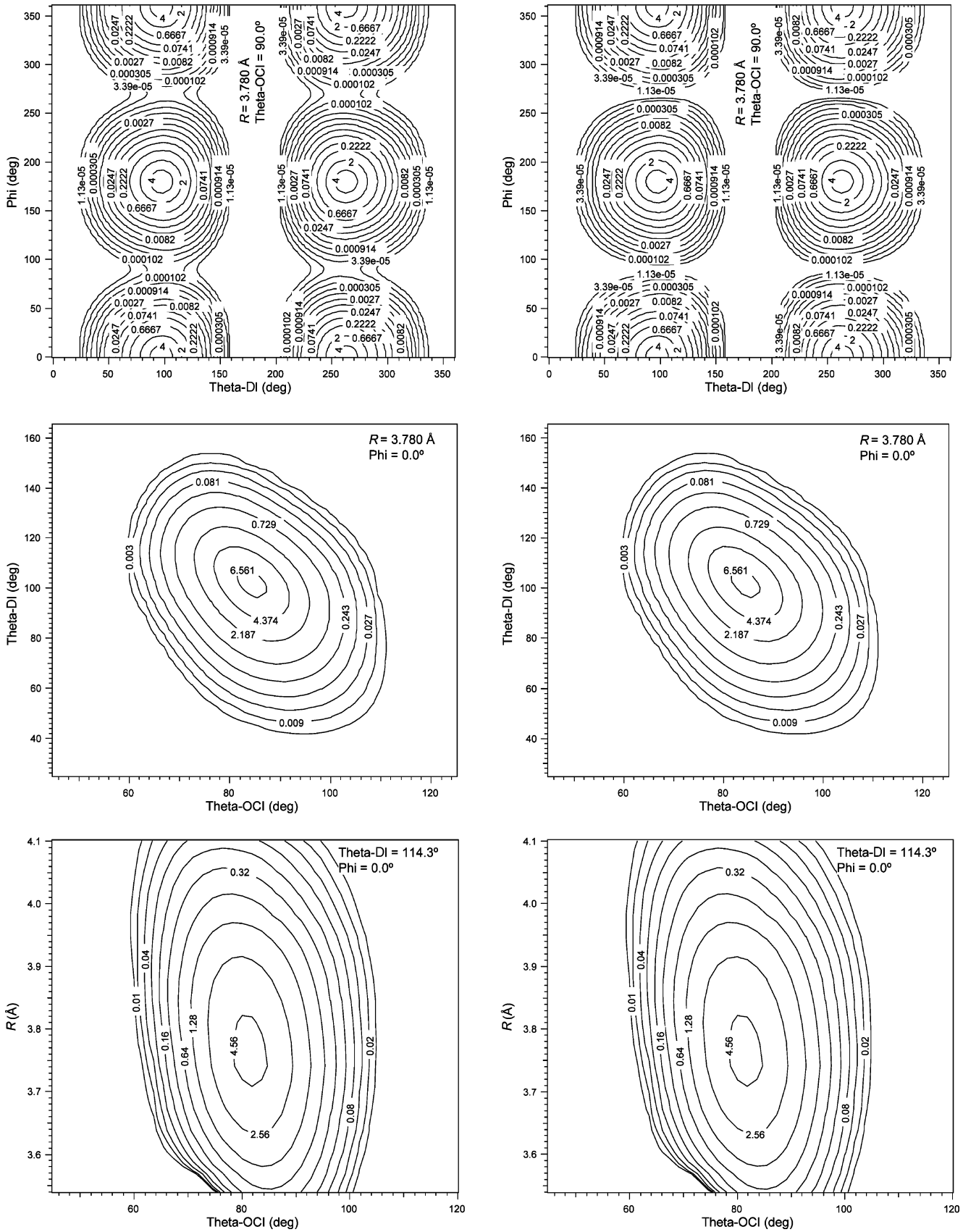

Figure 5. Probability densities of DI−$^{12}C^{16}O_2$ in the ground state (left side of the figure) with energy of $E = 361.687$ cm^{-1} and in the first excited state (right side of the figure) with energy of $E = 361.686$ cm^{-1}. All contours are given in arbitrary units.

$\phi = 0.0°$, and $R = 3.780$ Å, $\theta_{OCI} = 102.1°$, $\theta_{HI} = 114.3°$, $\phi = 180.0°$, separated by a barrier of 181(17) cm^{-1}. The top of the barrier was located at the geometry $R = 3.818$ Å, $\theta_{OCI} = 90.0°$, $\theta_{HI} = 98.1°$, $\phi = 90.0°$, which corresponds to a T-shaped geometry with the hydrogen located out-of-plane. Also the morphed potential has a secondary minimum with a well

depth of 405(14) cm^{-1}, at the geometry $R = 3.875$ Å, $\theta_{OCI} = 124.4°$, $\theta_{HI} = 35.4°$, $\phi = 0.0°$. The probability densities of HI−$^{12}C^{16}O_2$ for the ground state and first excited-state are given in Figure 4.

5. Discussion

In Section 3, the calculation of the angles θ_{CIH} and θ_{OCI} from our experimental results was discussed. This calculation led to a quasi-T-shaped geometry with two sets of supplementary angles. The morphed potential has been used to select the correct set of angles, shown on Figure 4, which correspond to the experimental values $\theta_{OCI} = 82.30(1)°$ and $\theta_{CIH} = 71.55(1)°$. In the previous analysis on HBr−CO_2[12], the angle θ_{CBrH} was determined by considering the experimental value of the D/H rotational constants, which implied that the proton was directed away from the CO_2 monomer. On the contrary, the present analysis indicates that the proton is directed toward the CO_2 unit in the HI−CO_2 complex. We could not observe lines for the DI−$^{12}C^{16}O_2$ complex. However, we were able to predict the values of the spectroscopic constants of DI−$^{12}C^{16}O_2$ based on the morphed potential (Table 6). The probability densities of DI−$^{12}C^{16}O_2$ for the ground state and first excited state are given in Figure 5.

In Table 2, we have compared the values of the rotational constant A of HI−$^{12}C^{16}O_2$ and HI−$^{12}C^{18}O_2$ with the values of the mono-^{18}O substituted complexes. It may be noticed that the values of A in HI−$^{12}C^{16}O_2$ and HI−$^{12}C^{18}O_2$ are significantly larger that those in the mono-^{18}O substituted complexes. This difference is not commensurate with an isotopic effect but can be interpreted as a consequence of the hindered rotation of the HI monomer in the HI−CO_2 complex. The hindered rotation of the HI monomer can occur via two significant pathways: in-plane and out-of-plane. On the basis of the morphed potential, the most probable pathway for the hindered rotation occurs out-of-plane, around the *a*-axis of the molecule as described by the angle ϕ (Figure 4). Along this pathway, the estimated height of the barrier is 181(17) cm^{-1}, which compares with the value of 184 cm^{-1} for HBr−CO_2.[12] This gives the following values for the frequency of tunneling through the barrier: 0.037 cm^{-1} for HI−$^{12}C^{16}O_2$, 0.035 cm^{-1} for HI−$^{12}C^{18}O_2$, and 0.001 cm^{-1} for DI−$^{12}C^{16}O_2$. As a consequence of the Bose−Einstein statistics of the spin-zero oxygen nuclei, only symmetric states were allowed for the ground vibrational state for even K_a and only antisymmetric states for odd K_a. Consequently, rotation-tunneling transitions were observed for the complexes HI−$^{12}C^{16}O_2$ and HI−$^{12}C^{18}O_2$. Thus, the observed discrepancy in the rotational constant A can be attributed to the allowed transitions in the symmetric complexes from the $K_a = 0$ symmetric state to the $K_a = 1$ antisymmetric state. Therefore, the rotational constant A for the symmetric complexes will have a larger magnitude by the value of the tunneling splitting, which was not directly determined in this experiment.

By using the value of the A rotational constant for the mono-^{18}O substituted complexes in eqs 12 and 13, it is possible to estimate the A rotational constant for both HI−$^{12}C^{16}O_2$ and HI−$^{12}C^{18}O_2$.

$$A(\mathrm{HI}-{}^{12}\mathrm{C}^{16}\mathrm{O}_2) = \frac{A(\mathrm{HI}-{}^{12}\mathrm{C}^{16}\mathrm{O}^{18}\mathrm{O}) \times I_{^{16}\mathrm{O}^{12}\mathrm{C}^{18}\mathrm{O}}}{I_{^{16}\mathrm{O}^{12}\mathrm{C}^{16}\mathrm{O}}} \quad (12)$$

$$A(\mathrm{HI}-{}^{12}\mathrm{C}^{18}\mathrm{O}_2) = \frac{A(\mathrm{HI}-{}^{12}\mathrm{C}^{16}\mathrm{O}^{18}\mathrm{O}) \times I_{^{16}\mathrm{O}^{12}\mathrm{C}^{18}\mathrm{O}}}{I_{^{18}\mathrm{O}^{12}\mathrm{C}^{18}\mathrm{O}}} \quad (13)$$

The calculated values for A are 11304.55(1) MHz (0.377(1) cm^{-1}) for HI−$^{12}C^{16}O_2$ and 10047.21(1) MHz (0.335(1) cm^{-1}) for HI−$^{12}C^{18}O_2$. With these values, the corresponding inertial defects are 2.23 and 2.00 uma·Å^2, respectively, which are close to the ones previously determined for the mono-^{18}O substituted complexes. It is also possible to estimate the tunneling frequencies, which are 1325.83(1) MHz (0.044(1) cm^{-1}) for HI−$^{12}C^{16}O_2$ and 1317.87(1) MHz (0.043(1) cm^{-1}) for HI−$^{12}C^{18}O_2$. These values can be compared with the tunneling frequency of HBr−CO_2[12] of 1200 MHz (0.040 cm^{-1}). The value of the θ_{OCI} angle can be reevaluated using eq 7 and the estimated A rotational constants with the tunneling frequency accounted for. The determined values are 82.30(1)° for HI−$^{12}C^{16}O_2$ and 82.51(1)° for HI−$^{12}C^{18}O_2$ (Table 3), in agreement with those determined for the mono-^{18}O substituted complexes. In the case of the mono-^{18}O substituted complexes, our morphed potential confirms the picture of pure rotational spectra observed in the experimental data. As the oxygen atoms are not equivalent, the tunneling does not occur.

We determined a minimum energy of 457(14) cm^{-1} for HI−CO_2 from the surface obtained with the optimized intermolecular potential. In the HX:CO_2 homologous series, values were obtained for CO_2−HF, CO_2−HCl, and HBr−CO_2, respectively, 837 cm^{-1}, 576 cm^{-1}, and 397 cm^{-1}, using a potential function developed by Muenter.[42] For HBr−CO_2, a full ab initio calculation at MP2 level provided a value of 392 cm^{-1}.[12] The dissociation energy D_0 was also obtained from our morphed potential, namely 340.954 cm^{-1}. For comparison, the dissociation energy for CO_2−HF was experimentally determined with a value of 672(4) cm^{-1},[43] and for CO_2−HCl, Oudejans et al. gave a rough estimate of 430 cm^{-1}.[44]

6. Conclusions

In the present work, the microwave spectrum of HI−CO_2 has been analyzed to obtain spectroscopic parameters and the geometry of this complex. The experimental data were used to morph the ab initio potential energy surface of HI−CO_2 in order to obtain an optimized intermolecular potential. The determined surface is characterized by two equivalent global minima with a well depth of 457(14) cm^{-1}, corresponding to the geometries $R = 3.780$ Å, $\theta_{OCI} = 77.9°$, $\theta_{HI} = 114.3°$, $\phi = 0.0°$, and $R = 3.780$ Å, $\theta_{OCI} = 102.1°$, $\theta_{HI} = 114.3°$, $\phi = 180.0°$, separated by a barrier of 181(17) cm^{-1}. Also, the morphed potential has a secondary minimum with a well depth of 405(14) cm^{-1} at the geometry $R = 3.875$ Å, $\theta_{OCI} = 124.4°$, $\theta_{HI} = 35.4°$, $\phi = 0.0°$. The determined structure is now available for interpreting regiospecific effects in photoinitiated reaction dynamics of the HI−CO_2 complex and its clusters.

The ground state geometry of the complex is planar, with the heavy atoms having a quasi-T-shape configuration, with geometry $\theta_{OCI} = 82.30(1)°$ and $\theta_{CIH} = 71.55(1)°$. This quasi-T-shaped geometry differs significantly from the one observed in HBr−CO_2[13] and the linear geometries found for CO_2−HCl[10] and CO_2−HF.[14] An interesting feature revealed by the morphed PES of HI−CO_2 is that the complex has a linear OCO−HI geometry when the separation of the monomers is large (i.e., $R = 6.000$ Å). In addition, when the distance between the monomers is shorter than the equilibrium distance (i.e., $R = 3.000$ Å), the complex has a T-shaped geometry with $\theta_{OCI} = 92.0°$, $\theta_{HI} = 96.1°$, and $\phi = 0.0°$. The model obtained in the present study is also directly relevant to furthering an understanding of photoinitiated H_nX:CO_2 complexes (X = I, Br, Cl, $n = 1$ and X = S, $n = 2$) reactions.

Acknowledgment. We gratefully acknowledge the financial support of the National Science Foundation through grants

DMS-0216275 and CHE-0613202 and as well as from CACE-(TAMU). John W. Bevan thanks the Robert A. Welch Foundation (grant no. A747) for financial support. We also thank Lisa M. Pérez for assistance in the ab initio calculations.

References and Notes

(1) Syage, J. A. *J. Phys. Chem.* **1995**, *99*, 5772.
(2) Buelow, S.; Radhakrishnan, G.; Catanzarite, J.; Wittig, C. *J. Chem. Phys.* **1985**, *83*, 444.
(3) Radhakrishnan, G.; Buelow, S.; Wittig, C. *J. Chem. Phys.* **1986**, *84*, 727.
(4) Scherer, N. F.; Khundkar, L. R.; Bernstein, R. B.; Zewail, A. H. *J. Chem. Phys.* **1987**, *87*, 1451.
(5) Rice, J.; Hoffmann, G.; Wittig, C. *J. Chem. Phys.* **1988**, *88*, 2841.
(6) Chen, Y.; Hoffmann, G.; Oh, D.; Wittig, C. *Chem. Phys. Lett.* **1989**, *159*, 426.
(7) Shin, S. K.; Chen, Y.; Oh, D.; Wittig, C. *Philos. Trans. R. Soc. London, Ser. A* **1990**, *332*, 361.
(8) Scherer, N. F.; Sipes, C.; Bernstein, R. B.; Zewail, A. H. *J. Chem. Phys.* **1990**, *92*, 5239.
(9) Ionov, S. I.; Brucker, G. A.; Jaques, C.; Valachovic, L.; Wittig, C. *J. Chem. Phys.* **1992**, *97*, 9486.
(10) Altman, R. S.; Marshall, M. D.; Klemperer, W. *J. Chem. Phys.* **1982**, *77*, 4344.
(11) Sharpe, S. W.; Zeng, Y. P.; Wittig, C.; Beaudet, R. A. *J. Chem. Phys.* **1990**, *92*, 943.
(12) Zeng, Y. P.; Sharpe, S. W.; Shin, S. K.; Wittig, C.; Beaudet, R. A. *J. Chem. Phys.* **1992**, *97*, 5392.
(13) Rice, J. K.; Lovas, F. J.; Fraser, G. T.; Suenram, R. D. *J. Chem. Phys.* **1995**, *103*, 3877.
(14) Baiocchi, F. A.; Dixon, T. A.; Joyner, C. H.; Klemperer, W. *J. Chem. Phys.* **1981**, *74*, 6544.
(15) Fushitani, M.; Shida, T.; Momose, T.; Räsänen, M. *J. Phys. Chem. A* **2000**, *104*, 3635.
(16) Soep, B.; Abbès, S.; Keller, A.; Visticot, J. P. *J. Chem. Phys.* **1992**, *96*, 440.
(17) Balle, T. J.; Flygare, W. H. *Rev. Sci. Instrum.* **1981**, *52*, 33.
(18) Suenram, R. D.; Grabow, J. U.; Zuban, A.; Leonov, I. *Rev. Sci. Instrum.* **1999**, *70*, 2127.
(19) McIntosh, A.; Wang, Z.; Castillo-Chará, J.; Lucchese, R. R.; Bevan, J. W.; Suenram, R. D. *J. Chem. Phys.* **1999**, *111*, 5764.
(20) Watson, J. K. G. *J. Chem. Phys.* **1967**, *46*, 1935.
(21) Gordy, W.; Cook, R. L. *Microwave Molecular Spectra*; Wiley: New York, 1984.
(22) Keenan, M. R.; Wozniak, D. B.; Flygare, W. H. *J. Chem. Phys.* **1981**, *75*, 631.
(23) Harris, S. J.; Janda, K. C.; Novick, S. E.; Klemperer, W. *J. Chem. Phys.* **1975**, *63*, 881.
(24) Steed, J. M.; Dixon, T. A.; Klemperer, W. *J. Chem. Phys.* **1979**, *70*, 4095.
(25) Leopold, K. R.; Fraser, G. T.; Klemperer, W. *J. Chem. Phys.* **1984**, *80*, 1039.
(26) Novick, S. E.; Davies, P.; Harris, S. J.; Klemperer, W. *J. Chem. Phys.* **1973**, *59*, 2273.
(27) Van Dijk, F. A.; Dymanus, A. *Chem. Phys. Lett.* **1968**, *2*, 235.
(28) McElmurry, B. A.; Lucchese, R. R.; Bevan, J. W.; Belov, S. P.; Leonov, I. I. *Chem. Phys. Lett.* **2005**, *407*, 40.
(29) Rivera-Rivera, L. A.; Lucchese, R. R.; Bevan, J. W. *Chem. Phys. Lett.* **2006**, *429*, 68.
(30) Huber, K. P.; Herzberg, G. *Molecular Spectra and Molecular Structure IV. Constants of Diatomic Molecules*; van Nostrand Reinhold: New York, 1979.
(31) González-Gaitano, G.; Isasi, J. R. *Chem. Educ.* **2001**, *6*, 362.
(32) Castillo-Chará, J.; Bevan, J. W.; Lucchese, R. R. *Comput. Phys. Commun.* **2002**, *145*, 48.
(33) Werner, H.-J.; Knowles, P. J.; Lindh, R.; Manby, F. R.; Schütz, M.; Celani, P.; Korona, T.; Rauhut, G.; Amos, R. D.; Bernhardsson, A.; Berning, A.; Cooper, D. L.; Deegan, M. J. O.; Dobbyn, A. J.; Eckert, F.; Hampel, C.; Hetzer, G.; Lloyd, A. W.; McNicholas, S. J.; Meyer, W.; Mura, M. E.; Nicklass, A.; Palmieri, P.; Pitzer, R.; Schumann, U.; Stoll, H.; Stone, A. J.; Tarroni, R.; Thorsteinsson, T. *MOLPRO, A Package of Ab Initio Programs*, 2006.1 ed.; Cardiff, U.K., 2006.
(34) Dunning, T. H., Jr. *J. Chem. Phys.* **1989**, *90*, 1007.
(35) Kendall, R. A.; Dunning, T. H., Jr. *J. Chem. Phys.* **1994**, *100*, 2975.
(36) Peterson, K. A.; Puzzarini, C. *Theor. Chem. Acc.* **2005**, *114*, 283.
(37) Boys, S. F.; Bernardi, F. *Mol. Phys.* **1970**, *19*, 553.
(38) Castillo-Chará, J.; McIntosh, A. L.; Wang, Z.; Lucchese, R. R.; Bevan, J. W. *J. Chem. Phys.* **2004**, *120*, 10426.
(39) De Lucia, F. C.; Helminger, P.; Gordy, W. *Phys. Rev. A* **1971**, *3*, 1849.
(40) Graner, G.; Rossetti, C.; Bailly, D. *Mol. Phys.* **1986**, *58*, 627.
(41) Castillo-Chará, J.; Lucchese, R. R.; Bevan, J. W. *J. Chem. Phys.* **2001**, *115*, 899.
(42) Muenter, J. S. *J. Chem. Phys.* **1995**, *103*, 1263.
(43) Oudejans, L.; Miller, R. E. *J. Chem. Phys.* **1998**, *109*, 3474.
(44) Oudejans, L.; Olson, D.; Miller, R. E. *J. Chem. Phys*. **1996**, *105*, 8515.